



NPRL3 loss alters neuronal morphology, mTOR localization, cortical lamination and seizure threshold

Philip H. Iffland II,¹ Mariah E. Everett,² Katherine M. Cobb-Pitstick,³ Lauren E. Bowser,² Allan E. Barnes,¹ Janice K. Babus,¹ Andrea J. Romanowski,¹ Marianna Baybis,¹ Soad Elziny,¹ Erik G. Puffenberger,² Claudia Gonzaga-Jauregui,⁴ Alexandros Pouloupoulos,¹ Vincent J. Carson² and Peter B. Crino¹

Mutations in nitrogen permease regulator-like 3 (NPRL3), a component of the GATOR1 complex within the mTOR pathway, are associated with epilepsy and malformations of cortical development. Little is known about the effects of NPRL3 loss on neuronal mTOR signalling and morphology, or cerebral cortical development and seizure susceptibility.

We report the clinical phenotypic spectrum of a founder NPRL3 pedigree (c.349delG, p.Glu117LysFS; $n = 133$) among Old Order Mennonites dating to 1727. Next, as a strategy to define the role of NPRL3 in cortical development, CRISPR/Cas9 *Nprl3* knockout in Neuro2a cells *in vitro* and in foetal mouse brain *in vivo* was used to assess the effects of *Nprl3* knockout on mTOR activation, subcellular mTOR localization, nutrient signalling, cell morphology and aggregation, cerebral cortical cytoarchitecture and network integrity. The NPRL3 pedigree exhibited an epilepsy penetrance of 28% and heterogeneous clinical phenotypes with a range of epilepsy semiologies, i.e. focal or generalized onset, brain imaging abnormalities, i.e. polymicrogyria, focal cortical dysplasia or normal imaging, and EEG findings, e.g. focal, multi-focal or generalized spikes, focal or generalized slowing. Whole exome analysis comparing a seizure-free group ($n = 37$) to those with epilepsy ($n = 24$) to search for gene modifiers for epilepsy did not identify a unique genetic modifier that explained the variability in seizure penetrance in this cohort. *Nprl3* knockout *in vitro* caused mTOR pathway hyperactivation, cell soma enlargement and the formation of cellular aggregates seen in time-lapse videos that were prevented with the mTOR inhibitors rapamycin or torin1. In *Nprl3* knockout cells, mTOR remained localized on the lysosome in a constitutively active conformation, as evidenced by phosphorylation of ribosomal S6 and 4E-BP1 proteins, even under nutrient starvation (amino acid-free) conditions, demonstrating that *Nprl3* loss decouples mTOR activation from neuronal metabolic state. To model human malformations of cortical development associated with NPRL3 variants, we created a focal *Nprl3* knockout in foetal mouse cortex by *in utero* electroporation and found altered cortical lamination and white matter heterotopic neurons, effects which were prevented with rapamycin treatment. EEG recordings showed network hyperexcitability and reduced seizure threshold to pentylentetrazol treatment.

NPRL3 variants are linked to a highly variable clinical phenotype which we propose results from mTOR-dependent effects on cell structure, cortical development and network organization.

- 1 University of Maryland School of Medicine Departments of Neurology and Pharmacology, Baltimore, MD 21201, USA
- 2 Clinic for Special Children, Strasburg, PA 17579, USA
- 3 UPMC Children's Hospital of Pittsburgh Department of Neurology, Pittsburgh, PA 15224, USA
- 4 Regeneron Genetics Center, Regeneron Pharmaceuticals Inc., Tarrytown, New York, 10591, USA

Correspondence to: Peter B. Crino
Department of Neurology
University of Maryland School of Medicine
110 S. Paca St., Baltimore, MD 21201, USA
E-mail: pcrino@som.umaryland.edu

Keywords: GATOR1; mTOR; cortical malformations; focal cortical dysplasia; epilepsy

Abbreviations: 4E-BP1 = eukaryotic translation initiation factor 4E binding protein 1; AAF = amino acid-free; CFP = cyan fluorescent protein; C:Y = CFP to YFP ratio; FCD = focal cortical dysplasia; GATOR1 = GTPase-activating protein activity towards rags complex 1; GFP = green fluorescent protein; KO = knockout; MCD = malformation of cortical development; mTOR = mechanistic target of rapamycin; N2aC = neuro2a cells; PS6 = phospho-ribosomal S6; PTZ = pentylenetetrazol; S6 = ribosomal S6 protein; TORCAR = mTORC1 activity reporter; YFP = yellow fluorescent protein

Introduction

Germline and somatic variants in mTOR pathway genes are the most common causes of malformations of cortical development (MCD).¹ The mTOR pathway plays a pivotal role in cerebral cortical development² and mTOR pathway gene variants leading to constitutive mTOR activation ('mTORopathies') provide the presumed pathogenic mechanism for altered cortical cytoarchitecture. Focal cortical dysplasia II (FCDII) is an MCD highly associated with drug resistant seizures defined pathologically by disorganized cerebral cortical lamination, enlarged (cytomegalic) dysmorphic neurons and heterotopic neurons in the white matter.³ Variants in genes encoding components of the GTPase-activating protein (GAP)-activity towards Rags complex 1 (GATOR1), including DEP-domain containing 5 (DEPDC5), nitrogen permease regulator like-2 (NPRL2) and nitrogen permease regulator like-3 (NPRL3)^{4–6} are the most common mTOR pathway gene variants associated with FCDII⁷ and hemimegalencephaly, an MCD defined by hemispheric enlargement and FCDII histopathology.^{8,9}

In non-neural cells, the GATOR1 complex modulates mTOR pathway activity in response to intracellular amino acid levels by governing translocation of mTORC1 (mTOR complex 1, mTOR bound to raptor) to and from the lysosomal membrane.^{10,11} In nutrient replete conditions, GATOR1 is inhibited, releasing mTORC1 to physically interact with its binding partners on the lysosomal surface in an active conformation. However, when intracellular amino acids are low, GATOR1 prevents translocation of mTORC1 to the lysosomal surface (remaining cytoplasmic), thereby inhibiting mTOR activity.¹² GATOR1 subunits are highly expressed in brain^{13,14} and the effects of, for example, DEPDC5 variants on cell size, motility, firing and cortical lamination have been assayed in experimental models^{15–20} and human brain specimens.^{4,7} While human tissue studies show a link between NPRL3 variants, MCD and mTOR activation,^{7,15,21} few studies have investigated the role of NPRL3 in neuronal morphology, cortical lamination and cortical circuitry.

We report the largest and genealogically oldest known NPRL3 patient pedigree and show that despite a common founder variant, clinical findings among affected individuals were highly heterogeneous with a spectrum ranging from normal brain imaging to hemimegalencephaly and seizure freedom to drug-resistant epilepsy. As a strategy to define mechanisms for clinical phenotypic heterogeneity, exome analysis was performed in this cohort but did not identify a gene modifier for seizure phenotype suggesting autonomous effects of the NPRL3 variant. To assess the role of NPRL3 in foetal brain development, CRISPR/Cas9 knockout (KO) of *Nprl3* *in vitro* resulted in mTOR signalling hyperactivation and mTOR-dependent abnormalities in

cell size and subcellular translocation of mTOR to the lysosomal membrane. Focal *Nprl3* KO using *in utero* electroporation caused mTOR-dependent cortical lamination defects and increased seizure susceptibility, both of which were prevented by the mTOR inhibitor rapamycin.

Materials and methods

NPRL3 variants in the Mennonite community

The Clinic for Special Children (CSC) is located in Lancaster County, Pennsylvania, USA, an area home to a large number of Plain (Amish and Mennonite) families. The CSC also cares for patients of Plain descent from other areas throughout the US with large Plain settlements. Our Mennonite pedigree was ascertained in a prospective manner to capture the clinical and genetic status of several known NPRL3 families; through genealogical corroboration and/or cascade testing of relatives to known heterozygotes, the pedigree was expanded into one large pedigree.

NPRL3 heterozygotes ($n = 133$; c.349delG, p.Glu117LysFS) were identified from the Mennonite community (2016–20) through whole exome sequencing, targeted NPRL3 variant testing or the Plain Insight Panel, an extended carrier test developed for the Old Order Amish and Mennonite communities. Cascade testing of extended family members was used to identify further potential heterozygotes. Clinical phenotypes were determined through medical interviews (consented over the phone or in writing) with parents of affected children (<18 years old) and adults (≥ 18 years old); six were excluded from the structured medical interview due to a dual genetic diagnosis, i.e. NPRL3 c.349delG heterozygotes who were known to have a second confirmed genetic condition associated with seizures, as the second condition might confound the aetiology of the seizure phenotype. For example, an individual who harboured heterozygous variants in NPRL3 and KRIT1 was not included in the analysis. Clinical MRI and EEG reports were retrospectively collected and analysed.

Association analyses were performed with whole exome sequencing data (Regeneron Genetics Center; RGC). Individual vcf files for each NPRL3 c.349delG heterozygote ($n = 83$) were parsed using FileMaker Pro (FMP) scripts and uploaded into a custom FMP database housing >4000 Amish and Mennonite exomes (SnPEff and ANNOVAR annotations). Exome variants ($n = 230\,656$) were filtered based on genotype quality (>98), allele balance (<2), minor allele frequency (>0.05) and a consistency check for Hardy-Weinberg equilibrium.

Exome sequencing

Exome sequencing was performed (at RGC; 22) in 1 µg of high-quality genomic DNA prepared for exome-captured libraries (NimbleGen VCRome SeqCap 2.1 or IDT XGen targeted capture reagent). Libraries were sequenced (Illumina HiSeq 2500 or the NovaSeq 6000 platforms) achieving coverage of >85% of bases at 20× or greater. Raw sequence reads were mapped and aligned to the GRCh38/hg38 human genome reference assembly using a cloud-based bioinformatics production pipeline that uses BWA-mem for mapping and alignment and GATK Haplo typeCaller for variant and genotype calling. Variants were annotated using an RGC implemented analysis and annotation pipeline that uses ANNOVAR and customized Perl scripts.

CRISPR/Cas9 construct generation and validation

Validated guide RNAs (gRNAs) targeting mouse *Nprl3* were calculated *in silico* using ChopChop software (chopchop.cbu.uib.no). Two gRNAs [*Nprl3* (A) and *Nprl3* (B)] targeting exon 5 of *Nprl3* were used for these experiments (Fig. 2A). A scramble gRNA sequence was used as a transfection and gRNA control. *Nprl3* sequence misalignments generated by CRISPR/Cas9 *Nprl3* editing were confirmed by sequencing (Supplementary material).

RT-qPCR was used to define changes in *Nprl3* mRNA expression after KO using three biological replicates of each line. Total RNA was extracted from cell pellets of *Nprl3* A and B KO lines, scramble and wild-type cells using the RNeasy Mini Kit. RNA was converted to cDNA using a high capacity cDNA reverse transcription kit. RT-qPCR was run using the following primers within *Nprl3* A/B edited regions: F = AGAAACCTAGTGGCAAGGAATG; R = ATCCTGAAGTGCTAGGATCAGC. Mouse GAPDH was used as an expression control (F = AGTCCGGTGTGAACGGATTTG; R = TGTAGACCATGTAGTTGAGGTCA). Using SYBR Power Green PCR master and primers described above, a standard dilution was created using wild-type cDNA at the following concentrations: 1:20, 1:60, 1:180, 1:540 and 1:1620. Negative controls used were DNase-free water and diluted random primers. Each sample was loaded into a MicroAmp optical 384-well reaction plate at 1:20 and topped with a MicroAmp adhesive film. Plates were assayed using a Viia7 qPCR machine. Analysis was performed as described previously.²²

Nprl3 knockout cell lines

Neuro2a cells (N2aC; Sigma-Aldrich) were transfected with CRISPR/Cas9-plasmid using Lipofectamine LTX with Plus reagent (Thermo Fisher Scientific) for 48 h. Transfected N2aC were assayed by flow cytometry (University of Maryland School of Medicine Flow Cytometry Core) sorting based on mCherry (Cas9) fluorescence. mCherry+ sorted cells were replated in complete media and grown to confluence.

Soma diameter

In vitro, cell soma diameter was measured in digital images²³ across the longest dimension of each soma (25 cells in each of two biological replicates). To define the mTOR-dependency of cell size changes, cells were incubated for 24 h with the mTOR inhibitors rapamycin (50 nM, Cell Signaling Technologies) or torin1, a highly selective mTORC1 and mTORC2 kinase inhibitor (50 nM, Tocris), using DMSO as a vehicle control (one-way ANOVA, $P < 0.05$).

In electroporated mouse pups (below), soma diameter was measured in green fluorescent protein (GFP)-labelled neurons in digital

images. The longest dimension of the soma was measured in 10 neurons from five different animals (50 total) for each experimental group (one-way ANOVA, $P < 0.05$).

Lysosomal mTORC1 activity

Cells were transfected with the cyan fluorescent protein/yellow fluorescent protein (CFP/YFP) FRET biosensor TORCAR (mTORC1 Activity Reporter), cultured for 24 h in complete DMEM imaging media and imaged on a Zeiss LSM Duo slit-scanning confocal microscope. Images at ×20 magnification recording CFP and YFP channel fluorescence were obtained using time-lapse imaging at 2-min intervals for 60 min. Following a 10-min baseline in complete imaging media, distinct experimental media, i.e. fresh complete media, amino acid-free (AAF) imaging media or complete media with torin1 (50 nM) were added ($n = 10$ cells per condition).

The CFP to YFP ratio (C:Y) was calculated for each cell and then averaged ($n = 10$ cells per group; Origin statistical software) within experimental groups, accounting for imaging focal plane fluctuations in living cells and differences in transfection efficiency. The percent change and statistical significance was determined using the average C:Y ratio during a 60-min baseline in complete media as the comparator for each experimental group (one-way ANOVA, $P < 0.05$).

Cell aggregation

Nprl3 KO, scramble and wild-type N2aC were plated at equal density into video dishes for 24 h. Video dishes were placed into an Olympus VivaView imaging incubator at 37°C with 5% CO₂. Three regions of interest (a ×4 magnification field) were selected in each of four video dishes (*Nprl3* A, *Nprl3* B, scramble and wild-type). Images were taken 10 times every 15 m for 48 h. Quantification of aggregate volume and number was defined in Bitplane using the surface tool. In separate experiments, rapamycin (50 nM) or torin1 (50 nM) was added to cell culture media immediately prior to imaging. Time-lapse images were compiled into videos for analysis.

Western assay

Cells were lysed in radioimmunoprecipitation assay (RIPA) buffer with protease and phosphatase inhibitors. Lysate supernatants were run on a Bolt BT Plus 4–12% gel (Invitrogen) and transferred onto PVDF membranes at 4°C. Membranes were probed overnight at 4°C with antibodies recognizing phospho-ribosomal S6 (PS6) or S6 ribosomal protein (mouse monoclonals; 1:500; Cell Signaling). β-actin (1:10 000, rabbit polyclonal; Abcam) was used to ensure equal protein loading. Blots were performed in triplicate using technical replicates for densitometry analysis (Origin software).

Immunocytochemistry and immunohistochemistry

Fixed N2aC were probed with primary antibodies: filamentous (F)-actin (1:1000; mouse monoclonal, Abcam), lysosome-associated membrane protein 2 (LAMP2; 1:1000; mouse monoclonal; Thermofisher), mTOR (1:1000; rabbit monoclonal; Abcam) or PS6 (Ser240/244; rabbit monoclonal; 1:1000; Cell Signaling). Secondary antibodies (Alexa Fluor488 or Alexa Fluor594; all 1:1000 dilution; Molecular Probes) were incubated with the cells for 2 h at room temperature.

Whole brains were post-fixed in 4% PFA overnight [12 h for post-natal Day 3 (P3) pups, 24 h for adult mice], paraffin embedded, microtome sectioned at 8 µm and probed with CTIP2 (1:500; rat

monoclonal; Abcam), GFP (1:1000; chicken polyclonal; Abcam), MAP2 (1:100; goat polyclonal; Abcam), PS6 (240/244) or ribosomal S6 protein (mouse monoclonals; 1:2000; Cell Signaling) primary antibodies and then secondary antibodies Alexa488, 647 and 594, respectively.

After staining, fluorescence intensity quantification was performed on adult mouse brains to define PS6 (240/244) levels. A far-red (Alexa 647) secondary antibody was used to probe for PS6 (240/244) due the limited overlap in the fluorescence emission spectrum with Alexa 488 (GFP). Z-stack images were taken on a spinning-disk confocal microscope and reconstructed in 3D using Bitplane software. Images were analysed in ImageJ by isolating the soma of an individual neuron and measuring the area and integrated density of the cell as well as the background fluorescence (also measured as integrated density) of each image. Mean, integrated density and background fluorescence were used to calculate the fluorescence intensity of PS6 (240/244) staining normalized to cell size and non-specific background fluorescence. Quantification of normalized fluorescence intensity data (arbitrary units; AU) was performed in Origin statistical software using ANOVA with a $P < 0.05$ deemed significant.

mTOR-lysosome co-localization analysis

N2aC lines were plated into chamber slides for 24 h, then incubated in AAF or complete media for 60 min. Fixed cells probed with mTOR and LAMP2 primary and secondary antibodies (below) were visualized on a spinning disk confocal microscope (Nikon). The fluorescence intensity of mTOR and LAMP2 was measured within a region of interest (ImageJ²³) reconstructed into a 3D-fluorescence intensity surface plot. mTOR and LAMP2 fluorescence intensity correlation was determined (Pearson's correlation coefficient, R) with the higher the correlation coefficient, the greater the degree of co-localization between mTOR and LAMP2.

In utero electroporation

Timed-pregnant CD1 mouse dams (Charles River) were anaesthetized at embryonic Day 14 (E14) using isoflurane anaesthesia and the uterine horns were surgically exposed as described previously.²⁴ Separate *Nprl3* (A) and *Nprl3* (B) plasmids (Golden Gate Assembly plus GFP) were micro-pipetted into the lateral ventricle of 3–7 embryos per dam. Electrode forceps were placed on either side of the embryo head and five electrical pulses were passed through the embryo to drive the plasmid into neural progenitors lining the telencephalic lateral ventricle. One cohort of dams was treated with a single rapamycin injection (1.0 mg/kg) at 24 h post-operatively. At postnatal Day 1 (P1), pups were examined under a dissecting microscope for GFP fluorescence through the skull. GFP-positive pups or littermate controls were selected for immunohistochemical analysis and euthanized at P3, or matured to 5 weeks for EEG implantation, seizure threshold testing and immunohistochemistry.

The greatest extent of electroporation, i.e. GFP fluorescence, was identified and three sections of this region from each animal were selected for analysis. Analysis of electroporated and control cortices was performed on 3D reconstructions of z-stack images taken on a spinning-disk confocal microscope. Regions of electroporation were matched across experimental groups to ensure similar brain regions were being assayed. The number of GFP positive neurons in cortical layers I–VI and the corpus callosum was quantified relative to the total number of GFP-positive cells within each section across groups. In addition, soma diameter was measured in layer II neurons in each experimental group.

EEG recording

EEG electrodes were implanted at 5 weeks of age and secured onto the skull 3 mm behind bregma under isoflurane anaesthesia. Continuous EEG recordings (48 h) were performed using the Pinnacle Technology 3 channel EEG system (Lawrence). Sirenia Seizure Pro software (Pinnacle Technology) was used to calculate line length as the sum of the absolute values between neighbouring data points over time and total EEG power defined as the total amount of activity across all frequency domains. Electroporated mice from dams with and without rapamycin treatment, or wild-type mice, were administered the pro-convulsant agent pentylenetetrazol (PTZ) at 55 mg/kg intraperitoneally²⁵ and recorded for 40 min to capture the time to first electrographic seizure detected by EEG. Forty minutes after PTZ injection, the experiment was terminated, and animals were euthanized using CO₂ asphyxiation and cervical dislocation. Latency to seizure was assessed manually using EEG recordings.

Statistical analysis

To determine NPRL3 variant expression in our patient cohort, surviving variants ($n = 57\,151$) were analysed using chi-square tests to assess differences in minor allele frequencies within the NPRL3 c.349delG cohort. The differences in the effects of *Nprl3* KO on S6 phosphorylation and cell soma diameter were determined using one-way ANOVA between groups, accepting a range of $P < 0.05$ to $P < 0.001$ as significant (see Fig. 2 legend). Analysis of eukaryotic translation initiation factor 4E binding protein 1 (4E-BP1) phosphorylation by fluorescence resonance energy transfer (FRET), mTOR/lysosome co-localization and assessment of differential effects of *Nprl3* KO on cell aggregation were assessed by one-way ANOVA. Differences in cortical lamination caused by *Nprl3* KO following *in utero* electroporation used ANOVA to define significant differences between cell counts in the cortex. Fluorescence intensity quantification of PS6 levels in adult mouse brain was statistically analysed using ANOVA with $P < 0.05$ deemed significant. Further statistical details on each experiment can be found in the appropriate results section and figure legends.

Study approval

This study was approved by the University of Maryland School of Medicine and Lancaster General Hospital Institutional Review Boards and Institutional Animal Care and Use Committees.

Data availability

The data supporting the findings of this study are available from the corresponding author upon reasonable request.

Results

NPRL3 pedigree

Of 133 NPRL3 mutation heterozygotes (NPRL3 c.349delG, p.Glu117LysFS; $n = 133$; Fig. 1 and Table 1), 48 (36.1%) had a history of seizures, while 85 had no seizure history. Of the 48 NPRL3 individuals with seizures, 42 completed structured medical interviews (six were excluded from interviews due to a dual genetic diagnosis). Affected individuals displayed markedly heterogeneous epilepsy phenotypes despite sharing the common founder NPRL3 variant. For example, the median age of seizure onset was 5 years but ranged from 1 day to 37 years. Clinical seizures subtypes included focal

Table 1 Summary of MRI and EEG findings in patients with NPRL3 variants

Subject ^a	Age at EEG, years	MRI findings			EEG findings					
		Normal	HME	FCD	Normal	Focal/multifocal IED	Focal seizure	Focal slowing	Generalized IED	Generalized slowing
1	0			+		+	+	+		
2	0	+				+	+		+	+
3	1	+				+				+
4	1			+			+			
5	1			+		+	+	+		+
6	3			+		+	+			
7	4			+		+	+			
8	4			+		+	+			
9	6	+				+	+			
10	6		+			+		+	+	+
11	6	+				+	+	+		+
12	7	+				+	+	+		
13	8	-	-	-		+				
14	8			+		+		+		
15	9	-	-	-	+					
16	9	+					+			
17	11	+				+	+	+	+	+
18	15			+		+	+	+		
19	20	-	-	-	+					
20	21	+					+			+
21	31	-	-	-			+			

A plus symbol indicates presence on MRI or EEG. Dashes indicate no data were available.

^aSubject numbers correspond to subject numbers in pedigree and MRI images in Fig. 1.

or generalized onset. Six individuals had a history of infantile spasms and one reported exclusively febrile seizures. The median peak clinical seizure frequency was 4.5 seizures per day but ranged from 4 per year to >20 per day. The median number of concurrent anti-seizure medications was 2 and ranged from 0 to 4. Within the cohort, the estimated penetrance of seizures was 28% (penetrance may be an underestimate as some patients may develop seizures later in life). Finally, while variants in *DEPDC5*, encoding a protein binding partner (*DEPDC5*) for NPRL3, have been associated with SUDEP,⁷ there were no reported SUDEP cases within our NPRL3 pedigree.

Available MRI data from 17 and EEG data for 21 NPRL3 mutation heterozygotes with epilepsy showed highly heterogeneous results (Fig. 1 and Table 1). MRI findings included normal brain structure in eight individuals and MCD in nine (FCD, eight and hemimegalencephaly, one). Nineteen EEGs showed both focal (spikes, sharp waves) and generalized (generalized spike and wave discharges, and/or slowing) abnormalities, while two individuals had normal EEGs (these had no MRI available). Interestingly, all cases with normal brain MRI had epileptiform EEG findings, i.e. inter-ictal or seizures; two cases where MRI was not available, had normal EEG. One individual in the pedigree with a single clinical seizure did not harbour the NPRL3 c.349delG variant.

Genetic modifiers of penetrance

We performed whole exome sequencing on all NPRL3 c.349delG heterozygotes to investigate whether any coding sequence variants affected seizure penetrance using a chi-square statistic comparing a seizure-free group ($n = 37$) to those with epilepsy ($n = 24$). Variants passing all filters and demonstrating significant chi-square values (>3.84) are found in Supplementary Table 1. Using both the chi-square statistic and the genotype classes, we failed to find a single

exome variant that could explain the differences in epilepsy penetrance in our NPRL3 c.349delG cohort.

mTOR pathway activation

Enhanced phosphorylation of ribosomal S6 protein (PS6; Ser240/244) has been reported in resected human NPRL3 brain tissue²¹ and in experimental models of *Nprl3* loss¹⁵ as a read-out for mTOR activation. We observed increased PS6 levels in lysates from two distinct *Nprl3* KO N2a cell lines (Fig. 2A and B) compared with scramble and wild-type cells. As expected, PS6 levels were reduced in *Nprl3* KO lines treated with the mTOR inhibitors rapamycin (150 nM) or torin1 (100 nM) (Fig. 2B). Next, since the GATOR1 complex inhibits mTOR activity in response to low cellular amino acid levels in non-neural cells, i.e. under conditions unfavourable for cell growth, we hypothesized that *Nprl3* KO would abrogate this effect of GATOR1 on mTOR in low amino acid conditions, resulting in persistent mTOR signalling. Indeed, while PS6 levels were reduced in scramble and wild-type N2aC grown in AAF media, PS6 levels remained elevated following *Nprl3* KO in AAF media (Fig. 2B). Thus, *Nprl3* KO alters GATOR1 function and is permissive to constitutive mTOR activation even when nutrient conditions are unfavourable for growth. Quantification of western assays and unedited blots can be found in Supplementary Fig. 1.

Increased soma size

Dysmorphic neurons in resected human FCDII tissue samples from epilepsy patients with NPRL3 variants are larger than control neurons.^{15,21} Thus, we hypothesized that *Nprl3* KO would result in mTOR-dependent increases in soma diameter. A 2-fold increase ($P < 0.001$) in soma diameter was observed in filamentous (F)-actin labelled *Nprl3* KO cells compared with wild-type N2a cells (50 cells per group; Fig. 2C and D). Rapamycin (50 nM) or torin1 (50 nM)

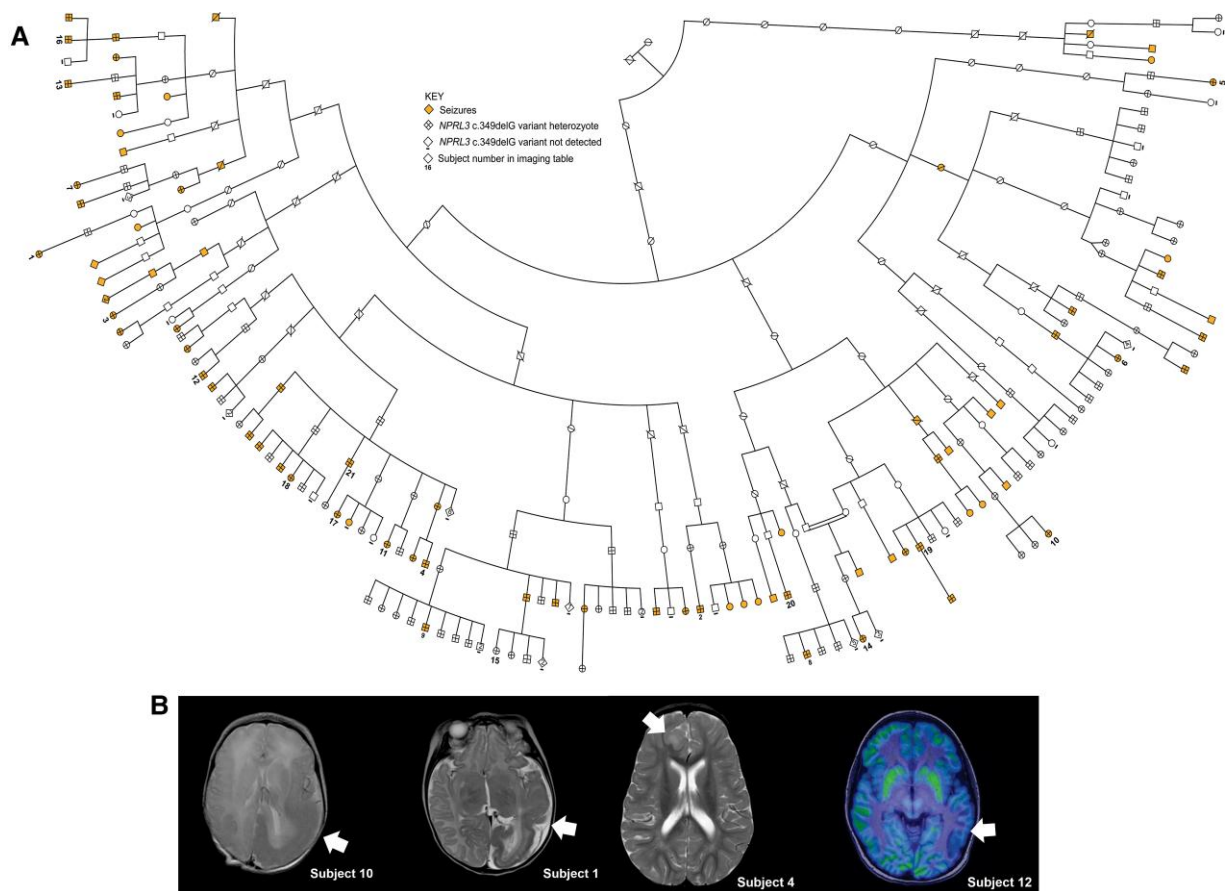


Figure 1 Old Order Mennonite pedigree with *NPRL3* founder mutation. (A) Proband ($n = 133$) heterozygous for the *NPRL3* c.349delG, p.Glu117LysFS variant. All patients were connected through a 12-generation pedigree to a founder mutation originating in an Old Order Mennonite couple from Pennsylvania born in 1727 and 1728. Heterozygous individuals are denoted with a cross-mark, while individuals in which the variant was not detected are denoted with a dash (-) below their symbol. Patients with seizures are denoted in orange. A number below a patient symbol corresponds to the subject number listed in C for EEG and MRI results. Of note, only one patient who did not have the *NPRL3* variant reported seizures. The number inside the diamond represents condensed sibling numbers to conserve pedigree space. (B) MRI and PET/MRI images for Subjects 10, 1, 4 and 12. Subject 10 at age 3 days, T₂-weighted image showing left hemimegalencephaly with associated cortical thickening (arrow). Subject 1 at age 7 weeks, T₂-weighted image showing large left hemispheric cortical dysplasia involving the parietal, temporal and occipital lobes (arrow). Subject 4 at age 1 year 7 months, T₂-weighted image showing focal cortical dysplasia in the right frontal lobe (arrow). Subject 12 at age 7 years 11 months, PET/MRI showing large area of hypometabolism in the left posterior temporal cortex in a patient without obvious focal cortical dysplasia on previous imaging (arrow). (C) MRI and EEG data (see text).

treatment for 24 h led to a reduction in soma diameter (Fig. 2D) equivalent to the wild-type ($P < 0.001$), demonstrating that enhanced cell size following *Nprl3* loss was mTOR-dependent.^{14,15}

Altered subcellular mTOR localization on the lysosome

When tethered to the lysosome, mTORC1 is active as a kinase. In non-neural cells, GATOR1 prevents translocation of mTORC1 to the lysosomal surface from the cytoplasm when intracellular amino acids are low,¹² i.e. conditions unfavourable for cell growth, thereby inhibiting mTOR activity; to date, this has not been studied in neurons. When conditions shift to nutrient deprived, GATOR1 shifts mTORC1 off of the lysosome to the cytoplasm to an inactive conformation.¹² In *Nprl3* KO N2aC (above), PS6 levels were not altered in AAF conditions demonstrating that the effects of *Nprl3* loss on GATOR1 modulation of mTOR signalling are not blocked by nutrient deprivation. Thus, we next investigated the effect of *Nprl3* KO on mTOR subcellular localization under AAF conditions, hypothesizing that *Nprl3* KO would result in persistent co-localization of mTOR on

the lysosome even under nutrient deprivation. *Nprl3* KO, scramble control and wild-type N2aC were incubated in complete or AAF media for 60 min, fixed, probed with anti-mTOR and anti-LAMP2 antibodies and imaged on a spinning-disk confocal microscope to define the correlation coefficient between mTOR and LAMP2 fluorescence intensity (Pearson's coefficient, R ; Fig. 3A). In complete media (nutrient replete conditions), there was a high correlation between mTOR and LAMP2 expression, with mTOR highly co-localized to the lysosome (Fig. 3A and B; $R \geq 0.9$ for each group; $n = 10$ per group). In contrast, mTOR dissociates from the lysosomal surface in wild-type and scramble N2aC in AAF media, evidenced by greater cytoplasmic mTOR localization ($P < 0.05$; R -values of 0.78 and 0.77, respectively, Fig. 3B). In *Nprl3* KO cells, mTOR and LAMP2 expression remained co-localized on the lysosome [$R = 0.89$ and 0.92 for *Nprl3* (A) and *Nprl3* (B), respectively] when incubated in AAF media. Thus, *Nprl3* KO allows mTOR to remain inappropriately localized to the lysosomal membrane in an activated conformation (evidenced by persistent phosphorylation of S6 protein, above) even under AAF conditions, demonstrating that *Nprl3* KO decouples mTOR subcellular localization and activation from modulation by metabolic state via GATOR1.¹⁰

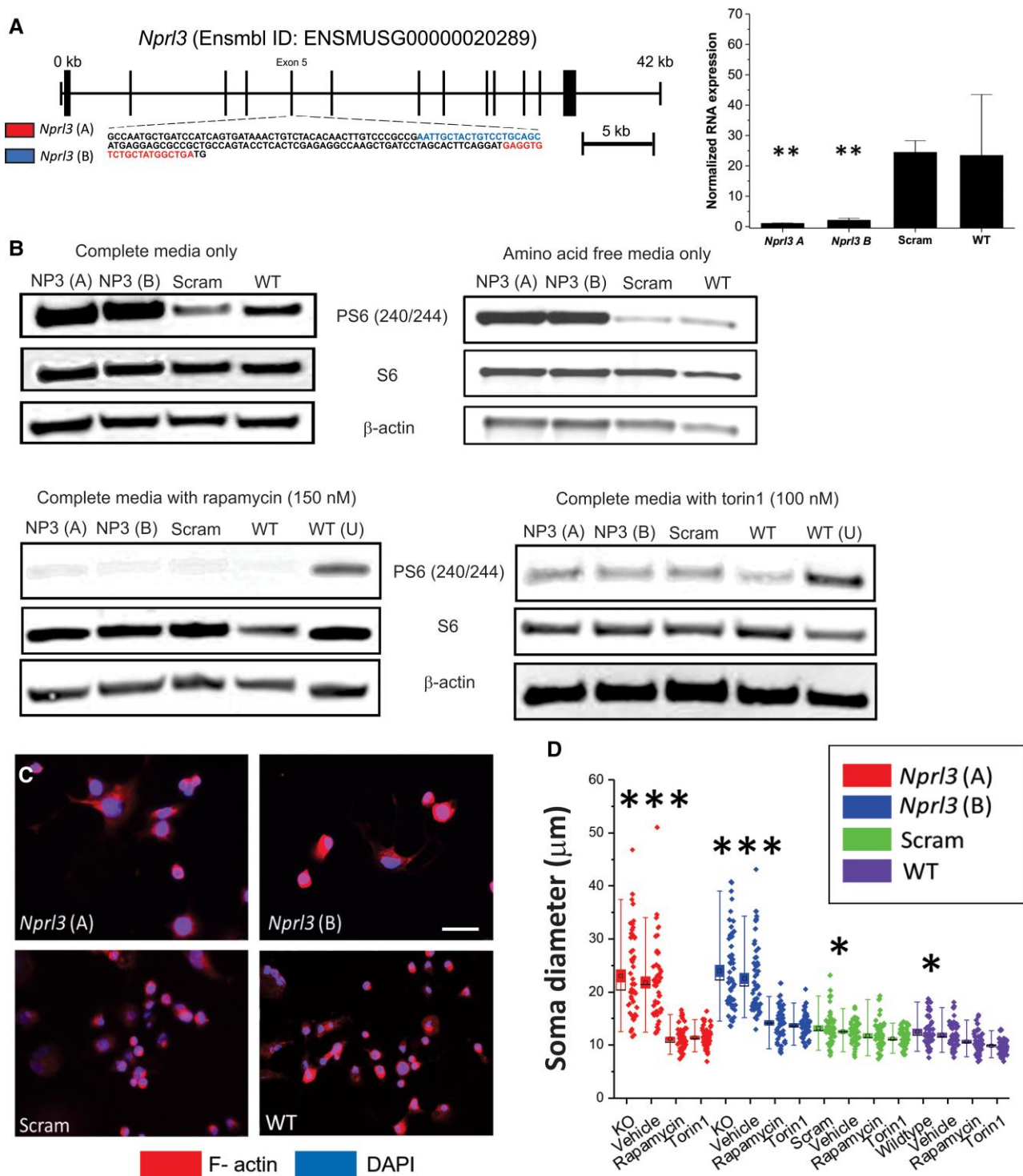


Figure 2 *Nprl3* KO results in mTOR-dependent increases in S6 phosphorylation and soma diameter. (A) *Nprl3* region targeted by in silico generated gRNAs targeting exon 5 of the mouse *Nprl3* gene. Vertical black bars represent exons with the thickness of each bar denoting relative size. Exon 5 PCR products assayed by whole amplicon next-generation sequencing showed sequence misalignments in both KO lines (Supplementary material). Bar graph shows RT-qPCR analysis revealing a decrease in *Nprl3* mRNA levels in KO lines. (B) Top: Increase in PS6 (240/244) in *Nprl3* KO N2aC in complete media that is reversed with rapamycin (150 nM, 60 min) or torin1 (100 nM; 60 min). Sustained levels of PS6 (240/244) were observed in *Nprl3* KO N2aC after incubation in AAF media versus scramble and wild-type (WT) cells (AAF media, 60 min). Unedited western blots and densitometry data for western assays can be found in Supplementary Fig. 1. (C) Representative images of each cell line are shown showing soma enlargement in *Nprl3* KO cells. (D) After *Nprl3* KO, a statistically significant increase in soma diameter was observed in *Nprl3* KO N2aC lines versus wild-type and scramble controls [$n = 25$ cells from each of two biological replicates (50 total cells per group); one-way ANOVA, $P < 0.001$]. Rapamycin (50 nM, 48 h) or torin1 (50 nM, 48 h), but not vehicle (DMSO), resulted in a statistically significant decrease in soma diameter in *Nprl3* KO N2aC; cell size was reduced by rapamycin and torin1 in control wild-type and scramble N2aC cells as well. In D, each box represents the SEM with a mean line shown, box whiskers represent the 5–95% confidence intervals, diamonds represent individual data-points. *** $P < 0.001$ versus scramble wild-type and torin1 or rapa, ** $P < 0.01$, * $P < 0.05$ versus torin1 and rapa. F-actin = filamentous actin; KO = untreated KO; NP3 = *Nprl3*; Scram = scramble; WT(U) = untreated wild-type lysate. Calibration mark in C = 25 μ m.

Activation of mTOR in live neurons at the lysosomal membrane

Phosphorylation of the mTOR substrate eukaryotic translation initiation factor 4E (eIF4E)-binding protein-1 (P4E-BP1; Thr36/47) serves as a measure of mTOR activation (akin to S6 protein, above). We used the CFP/YFP FRET biosensor TORCAR, which targets the lysosomal membrane via LAMP1 (like LAMP2, above, a lysosomal membrane protein), coupled to 4E-BP1.^{26,27} The ratio of CFP to YFP (C:Y) fluorescence provides a bioassay of dynamic changes in 4E-BP1 phosphorylation (increases or decreases) at the lysosomal surface in living cells. As 4E-BP1 phosphorylation is unaffected by rapamycin,^{28,29} TORCAR-transfected *Nprl3* KO, scramble, and wild-type N2aC were treated with torin1 in complete media for 1 h (Supplementary Fig. 3). The effects of torin1 are rapid, with progressive reduction in C:Y ratio, reflecting reduced P4E-BP1 levels, by 7.5% [*Nprl3* (A)] and 5.7% [*Nprl3* (B)] ($P < 0.001$; Fig. 3F and G) within 50 min (Supplementary Fig. 4). We next assayed the effects of nutrient deprivation. While scramble and wild-type N2aC incubated in AAF media exhibited an appropriate reduction in C:Y ratio (wild-type, 9.4% and scramble, 5.7%; $P < 0.001$; Fig. 3D and F), *Nprl3* KO N2aC lines showed persistent and inappropriate 4E-BP1 phosphorylation (Fig. 3D and F) unaltered by AAF exposure; this effect is similar to the S6 phosphorylation data above.

Together, the P4E-BP1 and PS6 data show mechanistically that *Nprl3* KO abrogates the effects of GATOR1 on mTOR subcellular localization and activation in response to nutrient deprivation, that nutrient deprivation cannot override the effects of *Nprl3* KO on mTOR activation, and importantly, that *Nprl3* KO drives mTOR activation over a range of metabolic conditions in neurons, decoupling mTOR from metabolic signalling.

Cellular aggregation

Human FCDII specimens exhibit cytomegalic dysmorphic neurons that may be observed occurring in close physical apposition (aggregates).³⁰ Interestingly, *Tsc1* KO astrocytes grow in clumps or aggregates *in vitro*,³¹ and a *Tsc2* KO mouse strain shows heterotopic cell clumps ('ring heterotopias') in the hippocampus.³² Since human NPRL3 variants are linked to FCDII histopathology, we hypothesized that *Nprl3* KO would cause abnormal cellular aggregation *in vitro*. N2aC typically grow in a monolayer with limited cell stacking *in vitro*. Thus, abnormal cellular aggregates were operationally defined using z-stack confocal imaging of closely apposed cells (no space between cell membranes) achieving an aggregate volume of $>200 \text{ mm}^3$. We first examined whether aggregates formed in live cells visualized by time-lapse bright-field imaging. *Nprl3* KO N2aC formed large aggregates ('clumps', mean volume 600 mm^3 ; Fig. 4) that progressively grew by accumulating cells from the surrounding environment over the 48-h imaging epoch. Dynamic video analysis revealed cells readily adhering to, but not detaching from, aggregates (Supplementary Video 1). The formation of cell aggregates was prevented with rapamycin (50 nM) or torin1 (50 nM; Supplementary Videos 2 and 3) treatment for 48 h, and during treatment, cells were observed moving freely within the recorded region rather than sticking to growing aggregates. In contrast, cell aggregates were not noted in control lines (Supplementary Video 1 and Fig. 4); small accumulations ($<100 \text{ mm}^3$) of cells are typical of wild-type and scramble N2aC cells.

We next examined total aggregate volume, aggregate number and cell number within aggregates in *Nprl3* KO cells using spinning-disk confocal microscopy in 3D (Fig. 4). Aggregate volume ($n = 10$ per

group; Fig. 4B, inset) in *Nprl3* KO N2aC lines exceeded 600 mm^3 compared with scramble and wild-type lines (Fig. 4A). The total number of cell aggregates in *Nprl3* KO N2aC lines (>60 aggregates per region) was dramatically increased compared to control N2aC lines (Fig. 4B). The total number of cells in each aggregate was quantified by counting the nuclei in each aggregate ($n = 10$ aggregates per group) and revealed statistically significant increases in cell number in *Nprl3* KO N2aC lines versus scramble and wild-type N2aC controls (Fig. 4D). Increases in aggregate number, volume, and increases in cell number per aggregate in *Nprl3* KO cells were prevented with rapamycin (50 nM) or torin1 (50 nM), demonstrating that aberrant cell aggregation following *Nprl3* KO was mTOR-dependent (Fig. 4C–E). Of note, enhanced cell proliferation [determined via 5-ethynyl-2'-deoxyuridine (EdU) assay] was not observed (Supplementary Fig. 2). Thus, mTOR-dependent cell aggregate formation did not result from enhanced cell proliferation.

Nprl3 and cerebral cortex structure

To model the effect of NPRL3 gene inactivation in the developing human brain,³³ we used *in utero* electroporation to transfect *Nprl3* (A) and (B) gRNAs and Cas9/GFP plasmids into neuroglial progenitor cells in the telencephalic ventricular zone on E14. Pups were euthanized on P3 and brain sections were probed with anti-GFP antibodies to visualize cells with *Nprl3* KO. Anti-CTIP2 antibody co-labelling was used to define layer IV–VI neurons in *Nprl3* KO and scramble transfected neurons.

All GFP-labelled neurons were observed in layer II/III in scramble gRNA electroporated pups consistent with cell fate destination to layer II/III for progenitor cells born at E14. In contrast, numerous GFP-labelled neurons were observed in deeper cortical layers IV–VI and in the subcortical white matter in *Nprl3* KO P3 mouse pups ($n = 5$; Fig. 5A). Deep layer GFP-labelled neurons in *Nprl3* KO pups did not co-express CTIP2. We submit that since the time point at which we electroporated each pup (E14) yields neurons with a layer II/III identity, the lack of CTIP2 expression in heterotopic neurons suggests improper positioning of neurons in the white matter destined for layer II/III. GFP-labelled neurons in *Nprl3* KO pups were larger than in scramble transfected pups ($P < 0.0001$; Fig. 5A and C) commensurate with observations following *Nprl3* KO *in vitro* (Fig. 2).

We next assayed whether mTOR inhibition during corticogenesis would rescue the effects of *Nprl3* KO on cortical lamination while avoiding the need for ongoing treatment. Pregnant dams were treated with rapamycin (1.0 mg/kg; single dose intraperitoneally) 24 h after *in utero* electroporation surgery (~E15). The half-life of rapamycin is ~60 h, so a single dose at E15 will affect mTOR activation in neural progenitors until late stages of corticogenesis, i.e. E18. When assayed at P3, the laminar defects observed in *Nprl3* KO pup brain sections were rescued by rapamycin with the preponderance of GFP-labelled cells observed in the appropriate layer II/III position (Fig. 5B and C). Further histopathological examination of *Nprl3* KO pups revealed normalization of cell size in all *Nprl3* KO GFP-labelled cells to wild-type size.

Excitability and seizure threshold

In the 5 weeks prior to EEG electrode implantation, no behavioural seizures were observed during twice daily observation of electroporated mice. At 5 weeks post-electroporation, dural electrodes were implanted over the electroporated cortical regions. EEGs were recorded for 48 h and no spontaneous seizures were observed in *Nprl3* KO or scramble control mice ($n = 6$ per group). To define subtle

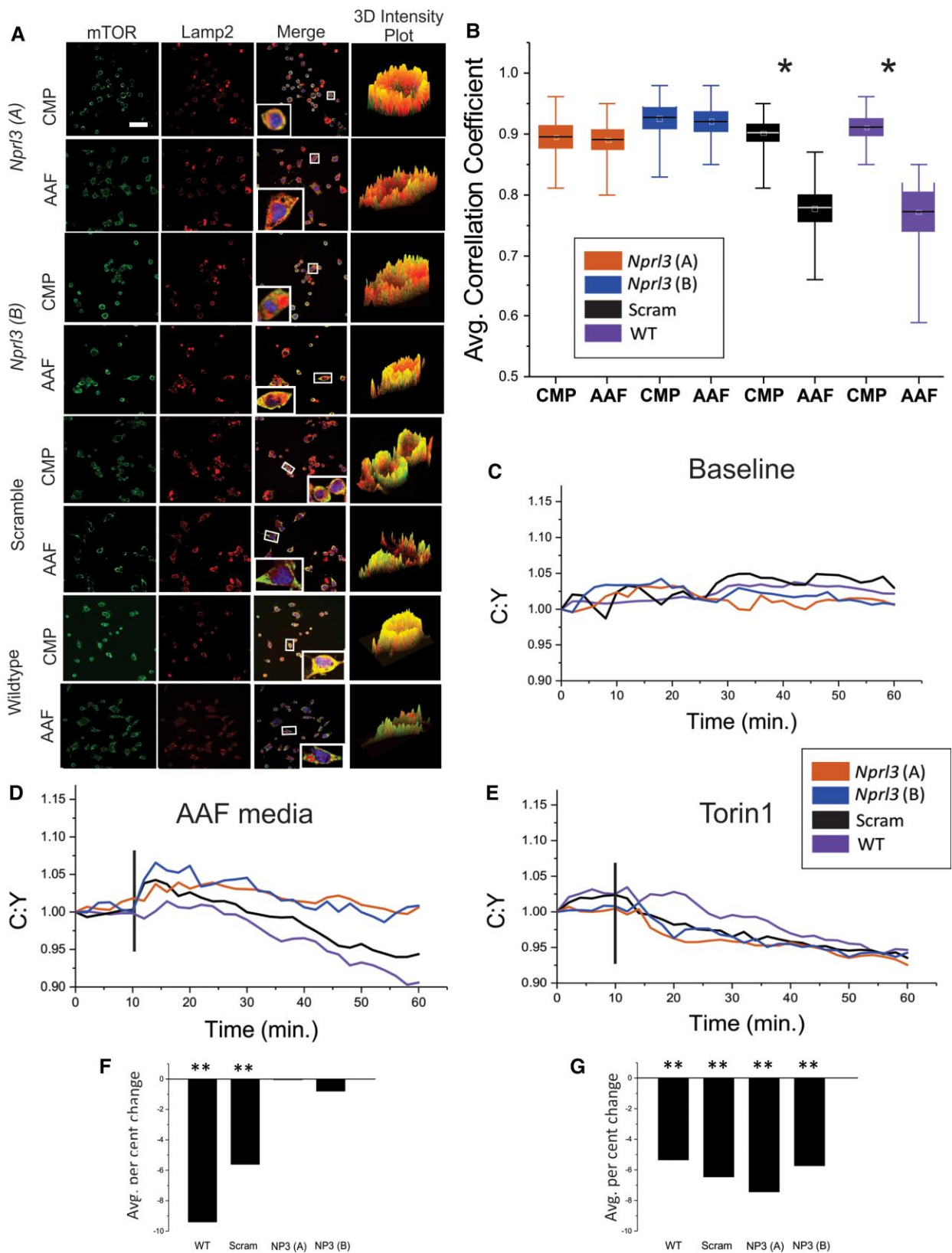


Figure 3 *Nprl3* KO alters mTOR subcellular localization on the lysosome and 4E-BP1 phosphorylation in living cells. (A) Co-localization regions of interest (representative regions of interest are shown as insets in A) between mTOR and LAMP2 are orange/yellow in 3D intensity plots, and regions of interest where mTOR and LAMP2 are not co-localized appear as distinct red and green areas. mTOR and LAMP2 are highly co-localized in control N2a cells in complete media. (B) Graphic depiction of average correlation coefficients determined in A. Comparing complete and AAF media, wild-type (WT) and scramble cell lines display a statistically significant decrease ($P < 0.05$) in co-localization between mTOR and the lysosomal membrane (LAMP2), whereas

(Continued)

electrographic changes that may indicate seizure propensity, we extracted line length as a measure of signal amplitudes, and total EEG power data, a measure of frequency band activity, from continuous EEG recordings for left and right hemispheres of KO and wild-type animals. In the electroporated cortices of *Nprl3* KO mice, higher signal amplitudes, i.e. increased EEG activity, were observed compared with the non-electroporated hemisphere and wild-type mice (Fig. 5F). Increased line length (Fig. 5F; arrow) observed in the electroporated cortex did not correspond to increased line length in the contralateral cortex, and therefore increased cortical activity in the electroporated cortex was independent of activity in the contralateral cortex. In contrast, wild-type mice exhibited similar overall line length, and thus similar levels of cortical activity, in both left and right hemispheres (Fig. 5F). These data were further quantified by total power data that revealed an increase in EEG power in the electroporated hemisphere of *Nprl3* KO mice compared with the non-electroporated hemisphere and wild-type mice (Fig. 5G). Rapamycin treatment after *Nprl3* KO rescued increased line length and total power seen in *Nprl3* KO hemispheres (Fig. 5F and G). Together, these data point towards an mTOR-dependent increase in cortical activity in *Nprl3* KO mice compared with the control.

Seizure threshold was assayed in mice injected with PTZ (55 mg/kg).³⁴ *Nprl3* KO mice displayed a significant decrease in seizure latency from time of PTZ injection to onset of first electrographic seizure (77.2 s, SEM = 11 s) compared with wild-type mice (168 s, SEM = 34 s; $P < 0.05$; Fig. 5H and I). Rapamycin treatment rescued seizure threshold as *Nprl3* KO pups from dams treated with rapamycin had a seizure threshold (latency) similar to wild-type mice (178 s, SEM = 52 s; Fig. 5H and I). Histological examination of implanted *Nprl3* KO cortices at 5 weeks post-*in utero* electroporation ($n = 6$) revealed that lamination defects, (GFP-labelled neurons in cortical layers IV–VI), persisted similar to P3 pups (Fig. 5E). Thus, mTOR inhibition rescued seizure threshold independent of cortical laminar abnormalities. Histological sections from 5-week-old *Nprl3* KO and wild-type littermate mice were also assayed for PS6 (240/244) levels using fluorescence intensity analysis ($n = 4$ per group). We observed a statistically significant increase in PS6(240/244) in GFP+ (KO) neurons while neurons within the electroporated region but not GFP+ has similar levels of PS6 fluorescence as wild-type littermate controls (Fig. 6; $P < 0.001$; $n = 30$ neurons per group). Total S6 levels were observed to be similar between GFP+ and adjacent GFP– neurons irrespective of PS6 (240/244) levels (Supplementary Fig. 5).

Discussion

We present the largest and oldest assembled founder NPRL3 pedigree reported to date originating within an Old Order Mennonite couple in the 1720s. As in non-Mennonite NPRL3 individuals,³³ there was a wide spectrum of clinical seizure phenotypes, EEG features and MRI findings, despite a common genotype in our cohort. As a strategy to understand how NPRL3 loss causes these phenotypes, we show that *Nprl3* KO induces mTOR-dependent increases in soma diameter both *in vitro* and *in vivo*. We demonstrate for the first time in neurons the effects of *Nprl3* KO on GATOR1 modulation

of mTOR in low nutrient conditions and show a mechanism by which mTOR remains activated following *Nprl3* KO, i.e. persistent localization of mTOR to the lysosome even under nutrient deprived conditions. A unique feature of *Nprl3* loss *in vitro* is enhanced cellular aggregation, prevented with mTOR inhibition. Focal *Nprl3* KO in foetal mouse brain *in vivo* causes results in heterotopic neurons in the white matter and reduced PTZ-induced seizure thresholds, both phenotypes that were rapamycin-sensitive. Importantly, our results are bolstered by findings in mice lacking *Depdc5*,^{16,17} suggesting a mechanistic association between DEPDC5 and NPRL3, known protein binding partners within GATOR1.

The penetrance of epilepsy in our cohort was 28%. In NPRL3 patients with epilepsy, MRI findings revealed a spectrum ranging from no visible abnormalities to hemimegalencephaly, ours being only the second reported case of hemimegalencephaly associated with NPRL3.⁹ Interestingly, the most severe seizure phenotypes were not always observed in patients with the most abnormal MRIs and in some individuals with seizures, brain MRI was normal suggesting either microscopic structural changes in the cortex or potentially, autonomous effects of NPRL3 loss on network excitability.

As a strategy to understand phenotypic variability, we reasoned that our large pedigree with common Mennonite haplotype background provided a unique opportunity to assess the effects of a modifier gene on seizure penetrance as, to date, no study has assessed genetic modifiers as a cause for clinical heterogeneity in MCD and epilepsy in mTORopathies. We readily acknowledge that whole genome sequencing would give the most comprehensive picture of gene modifiers for seizure phenotype within the genetic context of a founder NPRL3 mutation. Virtually all patients evaluated at the CSC undergo whole-exome sequencing, so we used this remarkable resource to seek exonic variants that might alter seizure phenotype. Our deep analysis did not yield single gene exon variants that might account for differences in seizure phenotype across this NPRL3 c.349delG cohort. So, while we cannot definitively say that there were no gene modifiers detected ‘genome-wide’, we can with confidence say that no modifiers were detected within wholly sequenced exomes, a finding that has not been previously reported in mTORopathies. This approach enabled us to exclude additional pathogenic variants in genes associated with seizure phenotypes within the compared cohorts and exclude any single gene variants within the exome, a necessary first step given the nature of enriched alleles within founder populations. Future whole genomic and epigenomic studies will be useful approaches to identify genetic modifiers with smaller or additive effects to seizure phenotype expression. Of course, we acknowledge that multiple polygenic modifiers may act independently in each individual or sibship or that our sample size is too small to detect modifiers. However, our data suggest an alternate mechanism through which heterozygous NPRL3 genotypes result in partially penetrant and clinically heterogeneous phenotypes.⁴ Finally, in contrast to DEPDC5 variants, the Mennonite NPRL3 variant does not appear to be associated with SUDEP as there were no cases of

Figure 3 Continued

no change in co-localization was observed in *Nprl3* KO cells incubated in AAF media. Boxes represent results from one-way ANOVA, with mean and SEM, whiskers are 5–95% confidence intervals. In C–G, TORCAR transfected cells, FRET-based C:Y ratio representing 4E-BP1 phosphorylation quantified in *Nprl3* KO, scramble control and wild-type N2aC lines. Cells were incubated in AAF media or complete media containing torin1 for 50 min. Measurements were taken at 2-min intervals. Statistical significance was calculated in comparison with complete media baseline recordings in C. Decreases in C:Y (4E-BP1 phosphorylation) were observed in wild-type (–9.4%) and scramble (–5.7%) N2aC after incubation in AAF media ($P < 0.01$), but no change in C:Y was observed in *Nprl3* A/B KO lines (D and F). Inhibition of mTOR with torin1 resulted in a significant decrease in C:Y in all experimental groups (E and G; $P < 0.01$) and, unlike AAF media, torin1 treatment of *Nprl3* A/B KO lines resulted in 7.4% and 5.7% reductions in C:Y, respectively ($P < 0.01$; G). * $P < 0.05$, ** $P < 0.01$. CMP = complete media; NP3 (A) = *Nprl3* (A); NP3(B) = *Nprl3* (B); scram = scramble. Calibration mark in A = 25 μ M.

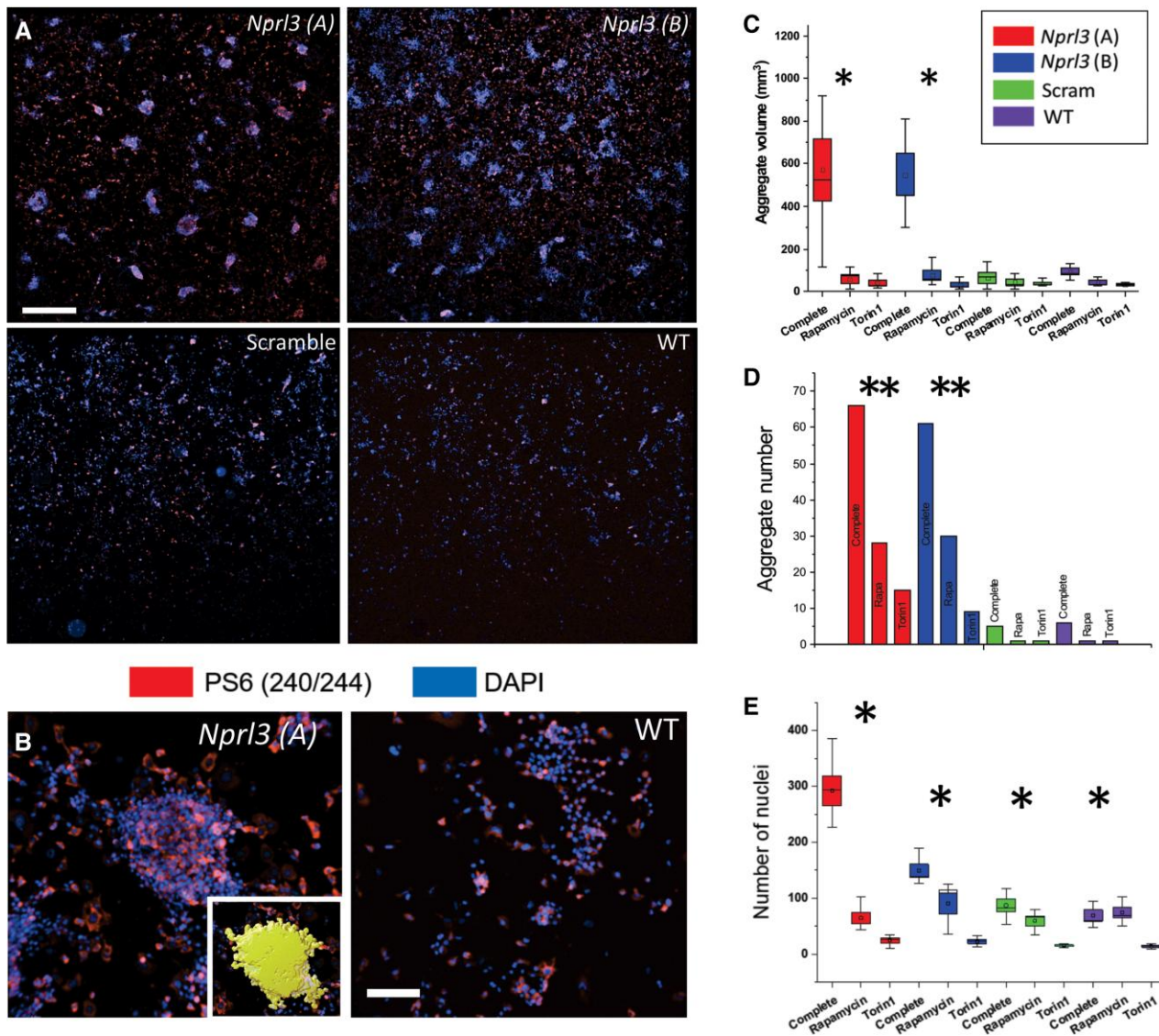


Figure 4 *Nprl3* KO results in mTOR-dependent cellular aggregation *in vitro*. (A) Representative confocal micrographs reveal large cellular aggregates in *Nprl3* KO lines but not control N2aC lines (time-lapse growth of aggregates visualized in [Supplementary Video 1](#)). Representative micrographs in B show high magnification image of a cellular aggregate in an *Nprl3* KO N2aC line compared with wild-type N2aC. The volume of each aggregate ($n = 5$ aggregates per group) in *Nprl3* KO N2aC lines is greater than in wild-type or scramble control N2aC (C; inset in B shows digital surface created to measure aggregate volume; $P < 0.05$). *Nprl3* KO N2aC have significantly increased total aggregate counts (D; $P < 0.01$). *Nprl3* KO aggregates have a greater cell number than control N2aC as measured by DAPI fluorescence (E; $P < 0.05$). Increases in aggregate number, volume, and cell number were prevented with rapamycin (50 nM; 48 h) or torin1 (50 nM; 48 h) treatment (C–E; see time-lapse imaging [Supplementary Videos 2 and 3](#)). ** $P < 0.01$, * $P < 0.05$. complete = complete physiological media; rapa = rapamycin; scram = scramble. Calibration mark in A = 500 μm . Calibration mark in B = 100 μm .

possible or confirmed SUDEP within this large cohort.⁷ Indeed, while sudden death was a phenotype observed in *Depdc5*-SynCre mice¹⁸ early death was not a feature in our mice after focal *Nprl3* KO.

We show that *Nprl3* KO resulted in persistent and inappropriate mTOR localization on the lysosomal membrane with ongoing signaling as evidenced by 4E-BP1 phosphorylation, even under nutrient deprived conditions. To date, no study has investigated lysosomal mTOR co-localization in living neurons or effects of a specific mTOR pathway gene on subcellular mTORC1 localization. Our data demonstrate that NPRL3 variants augment mTOR hyperactivation by allowing inappropriate and constitutive localization of mTORC1 to the lysosomal membrane in an active signalling conformation, even when unfavourable metabolic cellular demands require mTOR inhibition.^{10,15} The implications of these data are that loss of NPRL3 (and

potentially NPRL2 and DEPDC5) are fully permissive to constitutive mTOR signalling across a wide range of neuronal metabolic states.

Excessive cell aggregation is observed in models of tuberous sclerosis complex (TSC) including aggregation of *Tsc1* KO astrocytes *in vitro* and formation of ring heterotopias in *Tsc2* KO neurons *in vivo*.^{31,32} We show that *Nprl3* KO led to excessive and mTOR-dependent cellular aggregation *in vitro* prevented with rapamycin. In TSC, changes in cell adhesion molecule expression have been observed in human specimens^{35–37} that may explain increased cellular aggregation, e.g. expression of cell adhesion molecules may lead to enhanced adhesiveness of cells. Changes in cell adhesion could compromise neuronal motility during cortical development leading to altered cortical laminar organization.

In mice, focal *in utero* *Nprl3* KO led to neuronal enlargement and heterotopic neurons in white matter modelling several features of

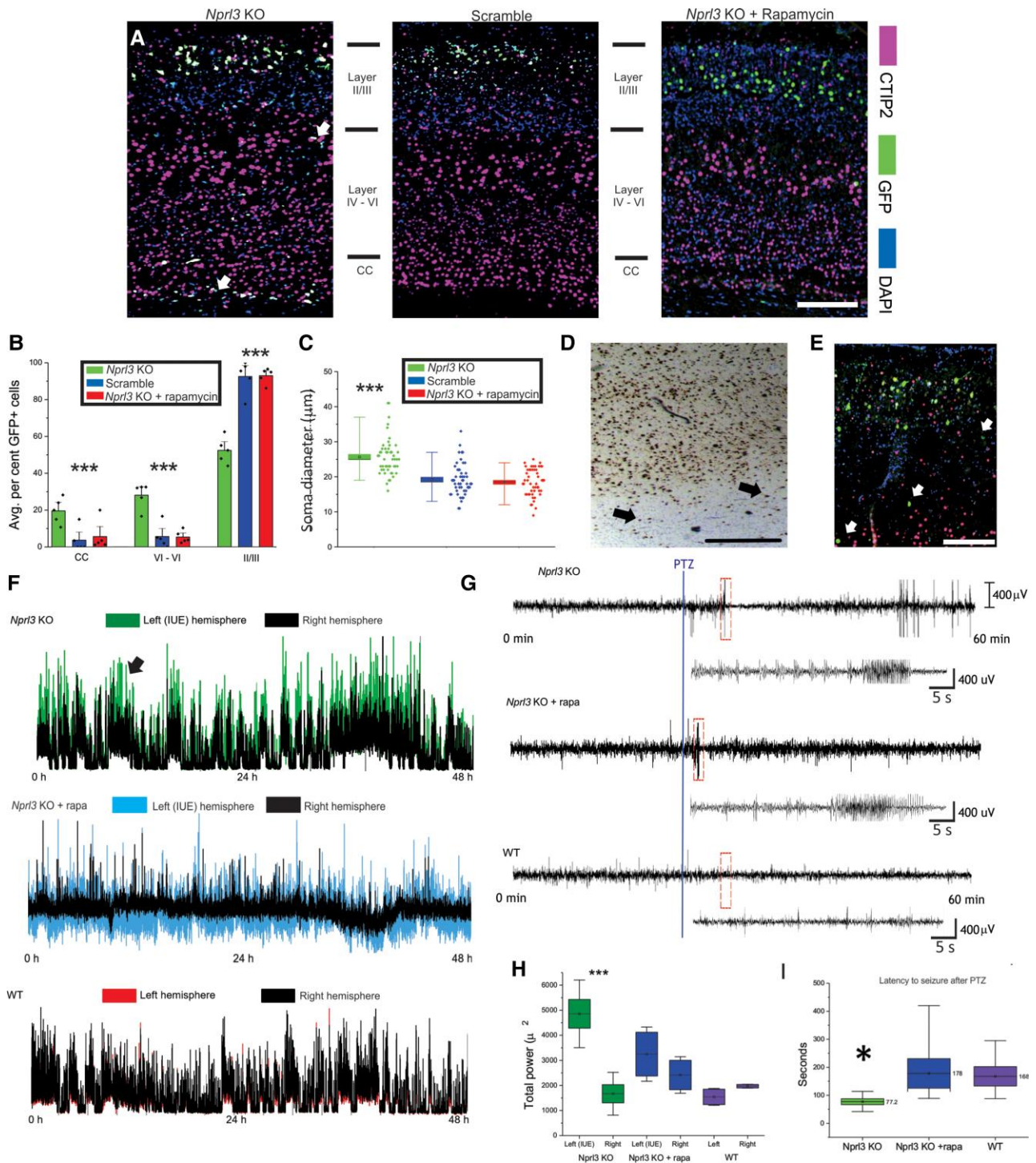


Figure 5 Focal *Nprl3* KO in vivo results in lamination defects, increased soma diameter, increased cortical excitability, and reduced seizure threshold. (A and B) GFP+ cells observed in the subcortical white matter (bottom arrow) and in layers IV-VI in *Nprl3* KO cortex at P3. In contrast, all GFP+ cells in scramble control specimens ($n = 5$ per groups; $P < 0.001$) were observed in the birthdate appropriate layer II/III. GFP+ neurons deep layers in *Nprl3* KO specimens did not express CTIP2 indicating that these cells had failed to attain their appropriate laminar destination in layers II/III. GFP+ cells in layer II/III in *Nprl3* KO pups were larger than scramble cells in the layer II/III. Rapamycin treatment prevented laminar defects (A and B) and soma diameter increases (C; each box represents mean, SEM, whiskers represent 5–95% confidence intervals). (D) Section from a surgical epilepsy FCD specimen (NeuN-labelled, from Subject 18 in Fig. 1) shows heterotopic white matter neurons (arrows) similar to what was observed in mouse (A and E, arrows). (F) Five weeks after in utero electroporation, mice were implanted with dural EEG electrodes and recorded for 48 h. A representative line length analysis of the 48 h EEG recording shows increased line length (a proxy for spike amplitude) in the electroporated cortex suggesting a hyperexcitable cortex ($n = 6$ per group) compared with the contralateral cortex and wild-type (WT) mouse cortices, where line lengths in the right and left hemispheres were similar. Total average EEG power also showed increased power in *Nprl3* KO cortices compared to the contralateral cortex and control cortices (G). Rapamycin treatment after *Nprl3* KO rescued increased line length and EEG power (F and G). Mice were treated with 55 mg/kg PTZ and EEGs were recorded. (H) Representative EEG tracings in *Nprl3* KO, *Nprl3* +rapamycin and wild-type mice. (I) After PTZ injection, *Nprl3* KO mice had a statistically significant average decrease (ANOVA; $P < 0.05$) in latency to seizure (77.2 s) compared with wild-type mice (168 s). Rapamycin treated *Nprl3* KO mice had seizure latencies that did not differ from control mice (178 s). *** $P < 0.001$, * $P < 0.05$. Calibration mark in A = 200 μ m.

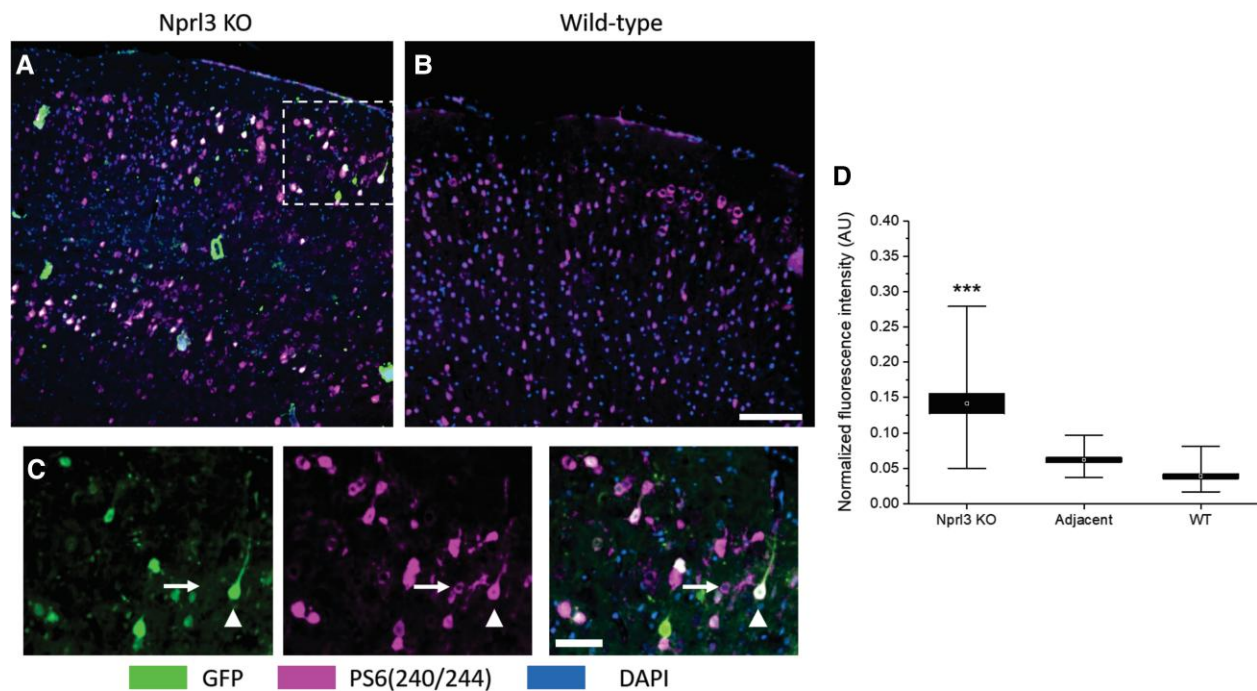


Figure 6 Focal *Nprl3* KO *in vivo* results in increased PS6 levels. In A and C, representative micrographs of 5-week-old *Nprl3* KO mouse brain and a wild-type littermate control are shown, respectively. PS6 (240/244) levels were measured in GFP+ neurons ($n = 30$ neurons per group). The dashed box in A demarcates the higher magnification area shown in B. In B, a GFP+ neuron (triangle) with increased levels of PS6 (240/244) is shown in comparison with an adjacent neuron (arrow; not GFP+) with lower levels of PS6. Measuring the fluorescent intensity of PS6+ neurons revealed a statistically significant (ANOVA; $P < 0.001$) increase in PS6 levels in *Nprl3* KO neurons compared to non-GFP+ neurons located within the electroporated region and to neurons from wild-type (WT) littermates (D). In D, boxes represent the SEM with a mean line shown, box whiskers represent the 5–95% confidence intervals. Total S6 levels were similar between *Nprl3* KO and adjacent non-GFP+ neurons (Supplementary Fig. 5). *** $P < 0.001$. Calibration mark in C = 200 μm , calibration mark in B = 50 μm . adjacent = non-GFP+ neurons adjacent to GFP+ neurons; AU = arbitrary units.

human *NPRL3*- and *DEPDC5*-associated FCD³⁸ and mouse *Depdc5* KO *in vivo*.^{16,17} Increased cell size (*in vitro* and *in vivo*) and laminar malpositioning were rescued with mTOR inhibitors. *NPRL3* and *DEPDC5* are functional binding partners within GATOR1 and may lead to similar, though not identical, histopathological phenotypes by mTOR-dependent mechanisms. While *Nprl3* KO did not result in spontaneous electrographic or behavioural seizures seen in a conditional mouse *Depdc5* KO strain or following *Depdc5* KO in rat,^{16,17} focal *Nprl3* KO (via *in utero* electroporation) and strain differences (rat versus mouse) could account for these disparities. However, we observed a decrease in seizure threshold in *Nprl3* KO mice suggesting that *Nprl3* KO led to a hyperexcitable network that was rescued by rapamycin.

Our data demonstrate new links between *Nprl3* KO and mTOR pathway hyperactivation, abnormal neuronal morphology, altered metabolic control of mTOR, disorganized cerebral cortical lamination, and enhanced seizure susceptibility that provides insights into the clinical phenotypic variability observed in *NPRL3* individuals. The absence of a detected modifier gene variant in this cohort argues that clinical phenotype is largely dictated by *NPRL3* loss. Importantly, we show that mTOR inhibition can rescue effects on cell and brain structure and network excitability caused by *Nprl3* KO and thus, these findings provide a pre-clinical platform for future studies examining the efficacy of mTOR inhibitors in patients with GATOR1 gene variants.

Acknowledgements

NPRL3 patients and their families; Dr Joseph Mauban, Manager of the University of Maryland School of Medicine Confocal Microscopy core, for his assistance with both live-cell slit-scanning

and spinning disk confocal microscopy; Dr Xiaoxuan Fan, Director of the Flow Cytometry Shared Service at the University of Maryland for his assistance in establishing CRISPR cell lines; Ryan Richardson at the University of Maryland School of Medicine for assistance in generating PX330 CRISPR plasmids; Philip H. Iffland, DDS for assistance with improving the EEG implantation technique; and Dr Jennifer Hopp, Epilepsy Division Director, University of Maryland School of Medicine, for EEG review. *Nprl3* sequence misalignments generated by CRISPR/Cas9 *Nprl3* editing were confirmed by Massachusetts General Hospital Center for Computational and Integrative Biology DNA Core for whole amplicon next-generation sequencing. TORCAR, courtesy of J. Zhang, Johns Hopkins University and Addgene plasmid # 64929; <http://n2t.net/addgene:64929>; RRID:Addgene_64929.

Funding

This work was supported by NIH NINDS R01NS099452 and R01NS094596 (PBC).

Competing interests

The authors report no competing interests.

Supplementary material

Supplementary material is available at *Brain* online.

References

- Crino PB. mTOR signaling in epilepsy: insights from malformations of cortical development. *Cold Spring Harb Perspect Med*. 2015;5(4):a022442.
- Osborne LR. Caveat mTOR: aberrant signaling disrupts corticogenesis. *J Clin Invest*. 2010;120(5):1392–1395.
- Iffland PH, Crino PB. Focal cortical dysplasia: Gene mutations, cell signaling, and therapeutic implications. *Annu Rev Pathol*. 2017;1/24(12):547–571.
- Baulac S. mTOR signaling pathway genes in focal epilepsies. *Prog Brain Res*. 2016;226:61–79.
- Baldassari S, Licchetta L, Tinuper P, Bisulli F, Pippucci T. GATOR1 complex: the common genetic actor in focal epilepsies. *J Med Genet*. 2016;53(8):503–510.
- Weckhuysen S, Marsan E, Lambrecq V, et al. Involvement of GATOR complex genes in familial focal epilepsies and focal cortical dysplasia. *Epilepsia*. 2016;57(6):994–1003.
- Baldassari S, Picard F, Verbeek NE, et al. The landscape of epilepsy-related GATOR1 variants. *Genet Med*. 2019;21(2):398–408.
- D’Gama AM, Woodworth MB, Hossain AA, et al. Somatic mutations activating the mTOR pathway in dorsal telencephalic progenitors cause a continuum of cortical dysplasias. *Cell Rep*. 2017;21(13):3754–3766.
- Canavati C, Klein KM, Afawi Z, et al. Inclusion of hemimegalencephaly into the phenotypic spectrum of NPRL3 pathogenic variants in familial focal epilepsy with variable foci. *Epilepsia*. 2019;60(6):e67–e73.
- Bar-Peled L, Chantranupong L, Cherniack AD, et al. A Tumor suppressor complex with GAP activity for the Rag GTPases that signal amino acid sufficiency to mTORC1. *Science*. 2013;340(6136):1100–1106.
- Sancak Y, Sabatini DM. Rag proteins regulate amino-acid-induced mTORC1 signalling. *Biochem Soc Trans*. 2009;37(Pt 1):289–290.
- Wolfson RL, Sabatini DM. The dawn of the age of amino acid sensors for the mTORC1 pathway. *Cell Metab*. 2017;26(2):301–309.
- Dibbens LM, de Vries B, Donatello S, et al. Mutations in DEPDC5 cause familial focal epilepsy with variable foci. *Nat Genet*. 2013;45(5):546–551.
- Yuskaitis CJ, Rossitto L-A, Gurnani S, Bainbridge E, Poduri A, Sahin M. Chronic mTORC1 inhibition rescues behavioral and biochemical deficits resulting from neuronal Depdc5 loss in mice. *Hum Mol Genet*. 2019;28(17):2952–2964.
- Iffland PH 2nd, Baybis M, Barnes AE, Leventer RJ, Lockhart PJ, Crino PB. DEPDC5 and NPRL3 modulate cell size, filopodial outgrowth, and localization of mTOR in neural progenitor cells and neurons. *Neurobiol Dis*. 2018;114:184–193.
- Hu S, Knowlton RC, Watson BO, et al. Somatic Depdc5 deletion recapitulates electroclinical features of human focal cortical dysplasia type IIA. *Ann Neurol*. 2018;84(1):140–146.
- Ribierre T, Deleuze C, Bacq A, et al. Second-hit mosaic mutation in mTORC1 repressor DEPDC5 causes focal cortical dysplasia-associated epilepsy. *J Clin Invest*. 2018;128(6):2452–2458.
- Yuskaitis CJ, Jones BM, Wolfson RL, et al. A mouse model of DEPDC5-related epilepsy: Neuronal loss of Depdc5 causes dysplastic and ectopic neurons, increased mTOR signaling, and seizure susceptibility. *Neurobiol Dis*. 2018;111:91–101.
- de Calbiac H, Dabacan A, Marsan E, et al. Depdc5 knockdown causes mTOR-dependent motor hyperactivity in zebrafish. *Ann Clin Transl Neurol*. 2018;5(5):510–523.
- Marsan E, Ishida S, Schramm A, et al. Depdc5 knockout rat: A novel model of mTORopathy. *Neurobiol Dis*. 2016;89:180–189.
- Ricos MG, Hodgson BL, Pippucci T, et al. Mutations in the mTOR pathway regulators NPRL2 and NPRL3 cause focal epilepsy. *Ann Neurol*. 2015;79(1):120–131.
- Nugent BM, Wright CL, Shetty AC, et al. Brain feminization requires active repression of masculinization via DNA methylation. *Nat Neurosci*. 2015;18(5):690–697.
- Schneider CA, Rasband WS, Eliceiri KW. NIH Image to ImageJ: 25 years of image analysis. *Nat Methods*. 2012;9(7):671–675.
- Parker WE, Orlova KA, Parker WH, et al. Rapamycin prevents seizures after depletion of STRADA in a rare neurodevelopmental disorder. *Sci Transl Med*. 2013;5(182):182ra53.
- Giardina WJ, Gasior M. Acute seizure tests in epilepsy research: electroshock- and chemical-induced convulsions in the mouse. *Curr Protoc Pharmacol*. 2009:Chapter 5:Unit 5 22.
- Zhou X, Clister TL, Lowry PR, Seldin MM, Wong GW, Zhang J. Dynamic visualization of mTORC1 activity in living cells. *Cell Rep*. 2015;10(10):1767–1777.
- Zhou X, Li S, Zhang J. Tracking the activity of mTORC1 in living cells using genetically encoded FRET-based biosensor TORCAR. *Curr Protoc Chem Biol*. 2016;8(4):225–233.
- Livingstone M, Bidinosti M. Rapamycin-insensitive mTORC1 activity controls eIF4E:4E-BP1 binding. *F1000Res*. 2012;1:4.
- Choo AY, Yoon SO, Kim SG, Roux PP, Blenis J. Rapamycin differentially inhibits S6Ks and 4E-BP1 to mediate cell-type-specific repression of mRNA translation. *Proc Natl Acad Sci U S A*. 2008;105(45):17414–17419.
- Urbach H, Scheffler B, Heinrichsmeier T, et al. Focal cortical dysplasia of Taylor’s balloon cell type: a clinicopathological entity with characteristic neuroimaging and histopathological features, and favorable postsurgical outcome. *Epilepsia*. 2002;43(1):33–40.
- Uhlmann EJ, Wong M, Baldwin RL, et al. Astrocyte-specific TSC1 conditional knockout mice exhibit abnormal neuronal organization and seizures. *Ann Neurol*. 2002;52(3):285–296.
- Way SW, McKenna J 3rd, Mietzsch U, Reith RM, Wu HC, Gambello MJ. Loss of Tsc2 in radial glia models the brain pathology of tuberous sclerosis complex in the mouse. *Hum Mol Genet*. 2009;18(7):1252–1265.
- Sim JC, Scerri T, Fanjul-Fernandez M, et al. Familial cortical dysplasia caused by mutation in the mammalian target of rapamycin regulator NPRL3. *Ann Neurol*. 2016;79(1):132–137.
- Claycomb RJ, Hewett SJ, Hewett JA. Prophylactic, prandial rofecoxib treatment lacks efficacy against acute PTZ-induced seizure generation and kindling acquisition. *Epilepsia*. 2011;52(2):273–283.
- Boer K, Crino PB, Gorter JA, et al. Gene expression analysis of tuberous sclerosis complex cortical tubers reveals increased expression of adhesion and inflammatory factors. *Brain Pathol*. 2010;20(4):704–719.
- Maldonado M, Baybis M, Newman D, et al. Expression of ICAM-1, TNF-alpha, NF kappa B, and MAP kinase in tubers of the tuberous sclerosis complex. *Neurobiol Dis*. 2003;14(2):279–290.
- Arai Y, Takashima S, Becker LE. CD44 expression in tuberous sclerosis. *Pathobiology*. 2000;68(2):87–92.
- Iffland PH 2nd, Carson V, Bordey A, Crino PB. GATORopathies: The role of amino acid regulatory gene mutations in epilepsy and cortical malformations. *Epilepsia*. 2019;60(11):2163–2173.